Solid state NMR characterization and flammability of styrene–acrylonitrile copolymer montmorillonite nanocomposite

Serge Bourbigot[a,*], David L. Vanderhart[b], Jeffrey W. Gilman[a,1], Séverine Bellayer[a,2], Holly Stretz[c], Donald R. Paul[d]

[a]*Fire Science Division, Building and Fire Research Laboratory, National Institute of Standards and Technology, Gaithersburg MD 20899, USA*
[b]*Polymers Division, Materials Science and Engineering Laboratory, National Institute of Standards and Technology, Gaithersburg, MD 20899, USA*
[c]*Texas State University, San Marcos, TX 78666, USA*
[d]*The University of Texas, Austin, TX 78712, USA*

Abstract

This work investigates the melt-processing of styrene–acrylonitrile copolymer (SAN) with organo-modified montmorillonite (MMT) clays and the influence of the clay on mechanical properties and on fire performance of SAN. The nanodispersion of MMT is evaluated qualitatively by X-ray diffraction (XRD) and transmission electronic microscopy (TEM), and quantitatively by solid state nuclear magnetic resonance (NMR). SAN/MMT nanocomposites reveal an intermediate morphology, an intercalated structure with some exfoliation and with the presence of small tactoids, whatever the loading in MMT is. The polymer–clay interfacial area is estimated at 0.5 and the degree of homogeneity characterizing the distribution of MMT platelets is about 40%. The presence of clay in SAN-25 leads to a 'filler effect' increasing the stiffness but decreasing tensile strength of the nanocomposites. It also leads to a significant decrease of peak of heat release rate measured by mass loss calorimetry.
© 2004 Elsevier Ltd. All rights reserved.

1. Introduction

Interest in polymer clay nanocomposites has increased significantly in recent years. The property improvements include better mechanical properties, better barrier properties, lower water absorption and reduced flammability [1–6]. To achieve these properties, mica-type layered silicates, such as montmorillonite (MMT), are generally dispersed at the nanoscale in the polymer to yield the so-called 'nanocomposite'.

The pioneering work of Gilman et al. has demonstrated that the presence of montmorillonite clay produces a substantial improvement in fire performance in polymeric matrices such as polystyrene and polyamides [5–7]. The purpose of this work is to investigate the melt-processing of styrene–acrylonitrile copolymer (SAN) with MMT clays and the influence of the clay on fire performance of SAN. In general, polymer clay composites are of three categories which are strongly dependent on the processing conditions (Fig. 1) [8–11]: microcomposites (Fig. 1(a)), exfoliated composites (Fig. 1(b)) and intercalated[3] composites (Fig. 1(c)). Many of the properties associated with polymer clay nanocomposites are a function of the extent of exfoliation of the individual clay sheets. Barrier properties, modulus,

---

* Corresponding author. Tel.: +33-3-20-43-48-88; fax: +33-3-20-43-65-84.

E-mail address: serge.bourbigot@ensc-lille.fr (S. Bourbigot).

[1] Present address: Laboratory PERF of Ecole Nationale Supérieure de Chimie de Lille, BP 108, 59652 Villeneuve d'Ascq Cedex, France.

[2] Guest Researcher from Laboratory GEMTEX of Ecole Nationale Supérieure des Arts et Industries Textiles (ENSAIT).

---

[3] The strict meaning of intercalculated is that the clay stack have swollen. The implication in this context is that swollen stacks would lead to a morphology intermediate between exfoliated and microcompressive, i.e. a mixture of nano-dimension stacks and single platelets. A microcomposite must then have a preponderance of stacks/tactoids that are micron in size.
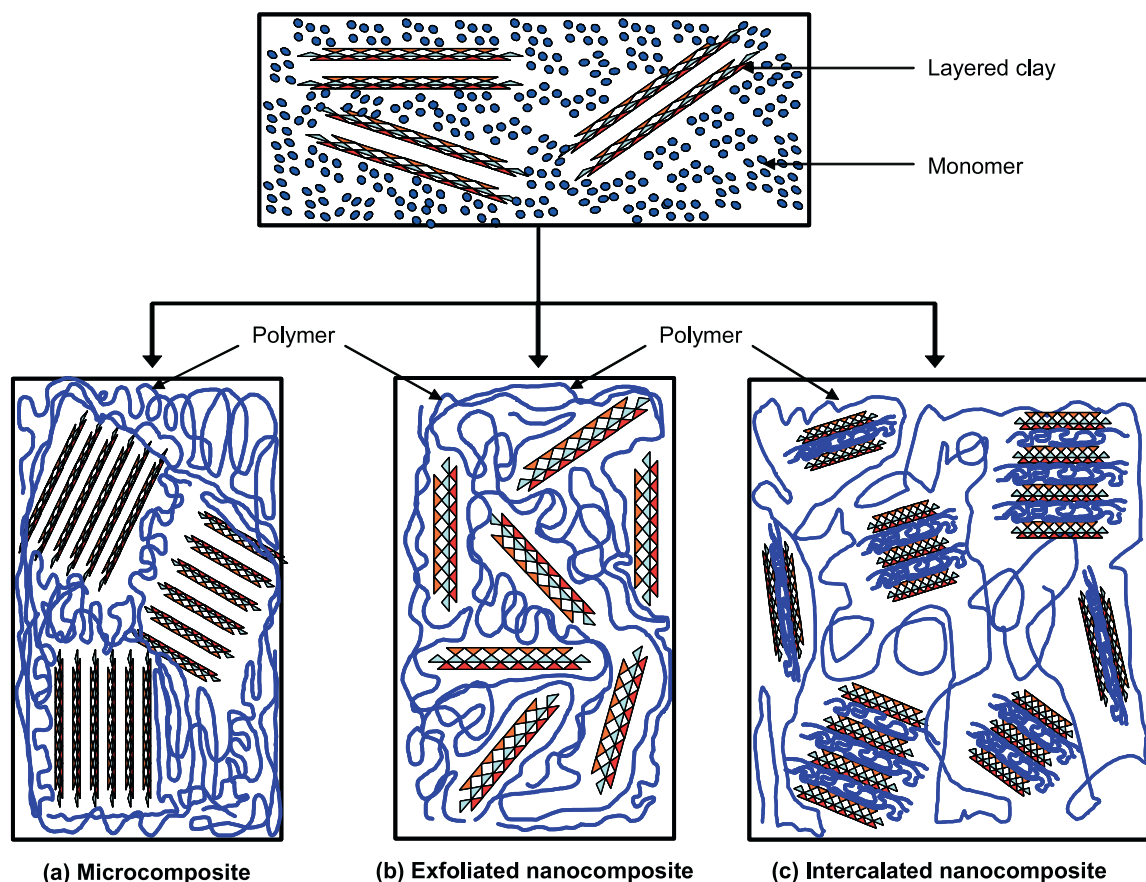
Fig. 1. Illustration of microcomposite (a) and of exfoliated (b) and intercalated (c) polymer clay nanocomposite morphologies. In this scheme, the nanocomposite is prepared by polymerization techniques from the monomer and from the organo-modified layered clay (the fraction of clay is exaggerated for illustrative purposes).

transparency and toughness have all been shown to be directly proportional to the degree of exfoliation, or the quality of the nanodispersion [1]. Nevertheless, the relation between exfoliated and intercalated morphology with respect to fire performance is not well established [12–15]. We recently suggested that no definitive relationship between 'nanostructure and fire performance' may be established without properly characterizing the nanodispersion (quantitatively speaking) in the polymer and using well calibrated samples (e.g. a purely exfoliated structure with a homogeneous distribution of MMT platelets) [15].

Our work is included in a large project aimed at understanding the flame retardancy of ABS. Computer housings are typically made from acrylonitrile–butadiene–styrene (ABS) polymer and related blends, and these polymers must meet safety standards. The SAN polymer discussed here is a model system for the study of ABS/clay systems, since the multi-phase ABS consists of an SAN matrix embedded with rubber particles. Our concern here is to simplify the system in order to study the nanodispersion of the clay in SAN. In addition, we will discuss in future publications how the clay dispersion and organoclay compatibilizer affect flammability in SAN and ABS.

Traditionally the dispersion of clay in a polymer is

characterized by transmission electron microscopy (TEM) and by X-ray diffraction (XRD) [16]. TEM and XRD provide essential information on the structure of the nanocomposite; TEM gives qualitative information and extensive imaging is required to insure a representative view of the whole material, while XRD allows quantification of changes in layered-silicate layer spacing. A new method has been developed at NIST to complement these nanocomposite characterization techniques. The method using solid state nuclear magnetic resonance (NMR) of protons is able to quantify the degree of nanodispersion of the layered-silicate in the bulk polymer [17]. The method is based on T_1^H (proton longitudinal relaxation time) measurement. The success of the method depends on two effects: (1) the paramagnetic character of the naturally occurring MMT (which directly reduces the T_1^H of nearby protons) and (2) spin diffusion, whereby this locally enhanced relaxation propagates to more distant protons [18–20]. The latter effect tends to prevent the method from being applied when dipolar interactions in the polymer matrix are too weak, i.e. when the polymer matrix is rubbery. Up to now, this method has been applied to polyamide-6 (PA-6) and polystyrene (PS) MMT nanocomposites exhibiting intercalated or exfoliated structures [17–20]. It is one of the goals in this

paper to extend the application of this method to SAN nanocomposites which have been prepared via melt blending and to quantify the degree of nanodispersion of the clay in the polymer.

The first part of the paper is devoted to the characterization by TEM of the nanocomposites. This should provide an overview of the dispersion of the clay in SAN. Then, we apply the NMR approach to quantify the degree of nanodispersion of the clay in SAN. Finally, tensile properties and flammability performance evaluated by mass loss calorimetry will be examined and discussed.

2. Experimental[4]

2.1. Preparation of the nanocomposites

MMT originated from Southern Clay Products, Inc (Gonzales, TX, USA). The starting material, sodium–MMT, was commercially modified using methyl, tallow, bis-2-hydroxyethyl, quaternary ammonium chloride (Cloisite 30B). SAN copolymer, containing 25 mass% (± 1 mass%) acrylonitrile (SAN-25) and formulated for computer housing, was supplied by Dow Chemical.

Polymer-melt direct intercalation is an approach to make polymer layered silicate nanocomposites by using conventional polymer extrusion. Processing temperatures could have an important effect on several potential mechanisms driving nanodispersion. Higher temperatures could be expected to increase the rate of collision of the polymer chains with galleries; increase degradation rates of the onium salt; reduce the melt viscosity; and reduce the surface tension of the melt. Clearly these factors could compete to either increase or reduce rates of exfoliation, leading to an optimum temperature. This effect is shown in Fig. 2 plotting Young's modulus (as an indicator of nanodispersion in the polymer) as a function of the melt extrusion temperature. According to the value of Young's modulus, it can be assumed that the best nanodispersion of the clay should be reached at 220 °C [21]. This temperature was adopted for the remainder of the study.

SAN-25 was melt-mixed with the clay using a co-rotating twin-screw extruder (Haake, screw $L/D = 10$, diameter = 35 mm) at 280 rpm. These conditions on this extruder have been shown previously to produce fully

---

exfoliated nylon-6/montmorillonite nanocomposites [22]. The clay loadings (Cloisite 30B) were 2.2, 4.2, 6.2 and 7.9 wt% true silicates. The true silicate concentration is determined by heating the dry, post-extrusion pellets in a muffle furnace to 900 °C for 45 min, and correcting for structural rearrangement by dividing the ash percentage by 0.935 (the silicate rearrangement results in 6.5% loss of structural water). Organoclay content can then be calculated from the true silicate content as reported here by using:

$$\text{organoclay (\%)} = \frac{0.935 \times MMT}{[1 - LoI/100]}$$

where LoI is the loss on ignition for the dry organoclay (30% for Cloisite 30B), and MMT is the true silicate weight percentage.

2.2. NMR spectroscopy

Measurements were conducted using a Bruker Avance 300 spectrometer (Bruker BioSpin Corp., Billerica, MA) operating at 7.05 T. Proton spectra at 300 MHz were obtained using a 5-mm low proton-background CRAMPS [22] (combined rotation and magic-angle spinning) probe (Doty Scientific of Columbia, SC).

It is known that the absorption of paramagnetic oxygen into aromatic polymers causes a major shortening of T_1^H [17, 24,25]. This effect becomes increasingly dominant with decreasing temperature. Thus, we measured the T_1^H's using deoxygenated samples. Deoxygenated granular samples were prepared by pumping at high vacuum for 1 h at 90 °C in 5 mm-OD glass tubes and sealing the tubes. T_1^H recovery curves were then measured using the saturation–recovery sequence with direct proton observation [26]. Three closely spaced 90° pulses accomplished the saturation. This sequence was preferred over the inversion-recovery sequence in order to minimize the number of experiments that would require long relaxation delays (five times the longest T_1^H). As a semiempirical approach to analysis, these saturation–recovery curves were fit to a two-exponential equation according to Eq. (1):

$$M(t) = M_{0s}(1 - e^{-t/T_{1s}^H}) + M_{0l}(1 - e^{-t/T_{1l}^H}) \tag{1}$$

where $M(t)$ is the magnetization at time t, M_{0s} and M_{0l} are the magnetizations of the short and long components, respectively, and, T_{1s}^H and T_{1l}^H are the proton longitudinal relaxation times of the short and long components, respectively, (see the discussion on the meaning of these two components in Ref. [17]). The equation was fit with the commercial program 'TableCurve2D' of Jandel Scientific using a standard least-squares minimization (Gaussian elimination). The accuracy of the fit was evaluated by an analysis of residuals in 95% confidence domain. All fitted values of T_{1l}^H and T_{1s}^H have 3 and 5% standard uncertainties, respectively. Corresponding standard uncertainties for the 2 M_0's are typically less than 5%.
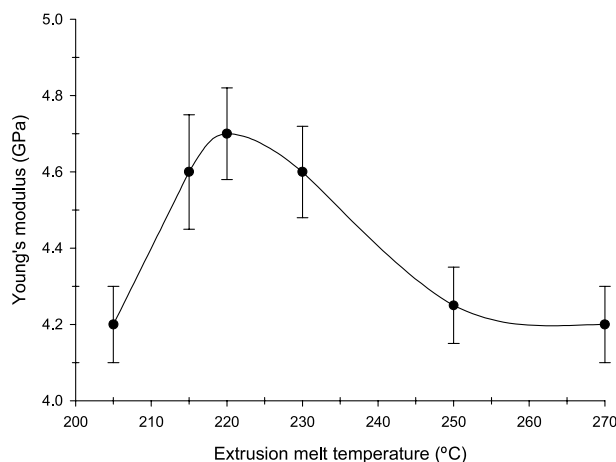
Fig. 2. Effect on processing temperature on Young's modulus of SAN-25/MMT nanocomposite.

Even though we recognized the strong effect of oxygen, T_1^H's of oxygen containing samples were obtained using the inversion-recovery sequence with direct proton observation [26] in a ZrO_2 rotor. For purposes of time efficiency, only the delay time, τ_{null}, was determined. The latter is the delay time where, after inversion, magnetization passes through zero on its way back to the Boltzmann equilibrium level. From τ_{null}, a lower limit for T_1^H was calculated via the relationship $T_1 = \tau_{null}/\ln 2$. This relationship assumes full initial inversion of the magnetization and single-exponential recovery. The paramagnetic contribution to T_1^H originating from the MMT clay normally produces a slightly accelerated early decay relative to the typically exponential behavior seen at longer times; hence, this relationship systematically yields a lower limit to the T_1^H that would describe this longer time behavior. In any case, all of the samples had equilibrated with O_2 and had aged for at least one month. Standard uncertainties for τ_{null} measurements are $\pm 2.5\%$ of those given value.

2.3. Transmission electron microscopy

All samples were ultra-microtomed with a diamond knife on a Leica Ultracut UCT microtome to give sections with a nominal thickness of 70 nm. The sections were transferred from water (room temperature) to Cu grids of 400 mesh. Bright-field TEM images of nanocomposites were obtained at 120 kV under low-dose conditions with a Philips 400T electron microscope, using Kodak SO-163 film. Low-magnification images were taken 22,000×. High-magnification images were taken at 100,000×. The materials were sampled by taking several images of various magnifications over 2–3 sections per grid to ensure that analysis was based on a representative region of the sample.

2.4. Tensile properties

Injection molding of tensile test bars (ASTM D638) was performed on an Arburg Allrounder 305-210-700 injection

molding machine. Test specimens were molded at a barrel temperature of 260 °C, and a mold temperature of 80 °C. Mechanical testing was performed on an Instron model 1137 at a strain rate of 0.51 cm/min, and moduli data were evaluated using an extensometer with a 2.5 cm gauge length. Standard deviations for 5 or more test bars were under 10% of the mean for moduli. Standard deviations on the tensile strength at break and strain at break increased with clay percentage up to a maximum of 15% of the mean.

2.5. Mass loss calorimetry by oxygen consumption

FTT (Fire Testing Technology) Mass Loss Calorimeter was used to carry out measurements on samples following the procedure defined in ASTM E 906. The equipment is identical to that used in oxygen consumption cone calorimetry (ASTM E-1354-90), except that a thermopile in the chimney is used to obtain heat release rate (HRR) rather than employing the oxygen consumption principle. Mass loss readings are performed simultaneously by ASTM E-1354, and serve as a benchmark of the HRR values obtained in this manner. ASTM E 906 is a screening method, and results in an internally representative set of data. Full scaleable HRRs from ASTM E-1354 are generally reported to be 2–3 times greater than values obtained here with the thermopile method for ABS materials. For comparison, fully scaleable peak HRRs from ASTM E-1354 for non-FR ABS grades range from 800 [27] to 1000 kW/m^2 [28] at an external heat flux of 35 kW/m^2.

Our procedure involved exposing specimens measuring $100 \times 100 \times 3$ mm^3 in horizontal orientation. External heat flux of 35 kW/m^2 was used for running the experiments. This flux corresponds to common heat flux in mild fire scenario [27–30]. The cone calorimeter was used to determine HRR. When measured at 35 kW/m^2, HRR is reproducible to within $\pm 10\%$. The cone data reported in this paper are the average of three replicated experiments.

3. Spin diffusion modeling in polymer/MMT nanocomposites

The direct influence of the paramagnetic Fe^{3+}, embedded in the aluminosilicate layers of the MMT, on polymer protons within about 1 nm from clay surfaces creates 'relaxation sources' which, via spin diffusion, significantly shorten the overall T_1^H. We used T_1^H as an indicator of the nanodispersion of the clay and spin diffusion modeling was used to describe this phenomenon and to quantify the degree of nanodispersion. The main expectation is that, for a given overall clay concentration, the better the dispersion of single MMT layers, the shorter is the average T_1^H. T_1^H measurements can, therefore, be used to probe the dispersion at the nano-scale of MMT in the polymer. This approach was fully described in one of our recent papers [17] and here, we will quickly remind the reader of the principles of the method.

Our approach is to simulate a spin-lattice relaxation experiment considering a very well exfoliated system (perfectly stratified system). The relevant equations are (see Ref. [31] for a full discussion on proton spin diffusion applied to polymer morphologies):

$$\frac{\partial P(r,t)}{\partial t} = \text{div}[D \cdot \overrightarrow{grad}(P(r,t))] + \frac{P_0 - P(r,t)}{T_1^H} \quad (2)$$

where $P(r,t)$ is the ensemble-averaged Zeeman polarization per spin, averaged over morphologically corresponding positions r and spin diffusion time t. P_0 is the average polarization per spin associated with Boltzmann-equilibrium; D is the spin diffusion coefficient (assumed to be a scalar and constant). The total spin magnetization, $M(t)$, which is proportional to the NMR signal intensity, can be obtained by integrating $P(r,t)$ over the region of interest Ω Eq. (3):

$$M(t) = \int_\Omega P(r,t)dr \quad (3)$$

The model [20] consists of two distinct domains (Fig. 3): the region of the paramagnetic source and the region of the polymer (SAN). To simplify the calculation, the assumptions are as follows: (a) the intrinsic T_1^H for the polymer layers in the nanocomposite is the spin diffusion averaged T_1^H of the pure polymer, (b) MMT platelets are parallel to one another and equally spaced (Δ is the platelet−platelet spacing), and (c) the paramagnetic influence of the Fe in the clay is replaced and mimicked by a fast-relaxing thin layer of SAN (we assume 0.4 nm as was done in the case PA-6 nanocomposite [20]) whose protons are in spin diffusion contact with the rest of the polymer. By modeling the problem as we have done, all we are creating is a relaxation source whose somewhat arbitrary width is tightly coupled to the relaxation time, $(T_1^H)_s$, assigned to this region in any fitting procedure.

Using a spin diffusion coefficient $D = 0.6$ nm^2/ms for the two regions [31,32], we will model both the spin diffusion

and the relaxation during a typical saturation recovery experiment. Before starting any computation, we need to estimate, Δ, the platelet−platelet spacing. Our model assumes a regular, repeating lamellar structure of alternating clay and PS; then the spacing can be calculated by $\Delta = (V_{clay}/V_{tot}d_{clay})^{-1}$ where V_{clay} and V_{tot} are, respectively, the fractional volume occupied, respectively, by the clay and the total volume in the nanocomposite. Hence, using a thickness, d_{clay}, of 1.0 nm for each clay layer, the densities of $\rho_{SAN} = 1.07$ g/cm^3 for SAN-25 and $\rho_{clay} = 2.83$ g/cm^3 for MMT, and mass fractions determined from TGA combustion residues (intentionally neglecting contributions from the organic modifier), then the spacing Δ can be estimated.

Using this approach, we introduced two concepts for analyzing the experimental recovery curves. These concepts are intended to answer two separate questions about the clay dispersion, namely, what fraction of the available clay layers form polymer–clay interfaces and, what is the homogeneity of the distribution of those polymer–clay surfaces that were formed?

For the first concept, we argued that in a plot of recovering magnetization vs. the square root of time, the initial slope corrected for the contribution from the intrinsic T_1^H of pure polymer, is nearly proportional to the total polymer–clay interfacial area. We then determined f, the fraction of 'effective' polymer clay interfacial area that did form relative to the maximum amount that could have formed. Also, from the initial slope of the calibration sample, one can establish $(T_1^H)_s$, the intrinsic relaxation time assigned to the 0.4 nm-wide interfacial region. $(T_1^H)_s$ was estimated at 2.5 ms.

The second concept is that the long T_1^H, i.e. T_{1l}^H, obtained from the biexponential fit to the experimental data can be matched, using our model calculation, to an apparent mean spacing, Δ_{app}, between clay–polymer interfaces. That is to say, after proper calibration, D and $(T_1^H)_s$ are fixed in the calculation, thereby leaving Δ_{app} as the only variable which defines the long T_1^H of the final slope. On the other hand, since we have also determined f and presumably know the clay concentration, we can also calculate an idealized spacing, Δ_f, corresponding to an idealized dispersion of the actual interfacial area. Then, the ratio of Δ_f/Δ_{app} will be a qualitative relative measure of the homogeneity of the dispersion of the actual surface area (hereafter called ε), i.e. ratios significantly less than unity imply poor dispersion of the available interfaces.

4. Results and discussion

This section is organized in a way that first, characterizes qualitatively the nanodispersion of clay in SAN-25 using usual methods (TEM and XRD). The second paragraph uses NMR to quantify the degree of nanodispersion in SAN-25. Then, tensile properties and flammability of these SAN-25 MMT nanocomposites are examined.
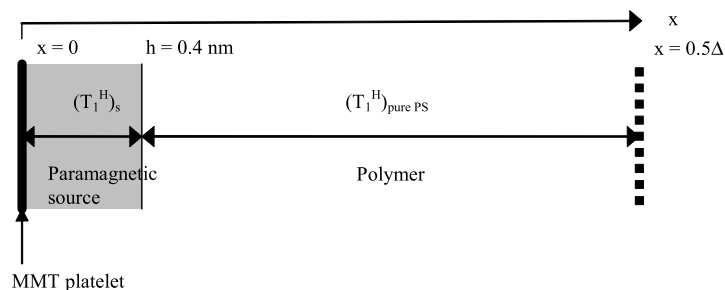
Fig. 3. One dimensional model simulating a perfect stratified system. Two regions can be distinguished; a narrow region experiencing direct paramagnetically-induced relaxation and a much broader region experiencing only indirect paramagnetically-induced relaxation. There is no polarization transport across the clay surface nor is there transport across the boundary at 0.5Δ owing to assumed symmetry.

4.1. Characterization by XRD and TEM

TEM images of SAN-25 MMT nanocomposites containing 2.2, 4.2, 6.2 and 7.9 wt% of true silicate are shown at low magnification (from Figs. 4(a)–7(a)) and at higher magnification (from Figs. 4(b)–7(b)). At low magnification, the images reveal that clay is well and evenly dispersed in all nanocomposites. At higher magnification, all samples exhibit dispersion of multi-layer stacks (tactoids) of individual MMT layers that range from 2 to 10 layers in size. Some individual MMT layers can be also distinguished. The samples are not all similar; the nanostructure of nanocomposite (size of the tactoids) appears qualitatively to be dependent on the loading in organoclay, although a quantitative analysis of the distribution has not yet been attempted (see the following for further discussion). We observe as the clay loading is increased, larger tactoids seems to become more prevalent. In addition to this, XRD spectra (not shown) [21] reveal diffraction peaks in the low angle region giving a d-spacing falling in between 3.1 and 3.25 nm. The d-spacing of the original organoclay is of

1.75 nm and this result suggests that at least a part of the nanocomposite has an intercalated structure. From TEM and XRD, we may conclude that the nanocomposites have mixed intercalated/exfoliated structure regardless of the loading.

4.2. Determination of the nano-mixing

Our theoretical approach (see the previous section and the full discussion in Ref. [17]) has shown that the first part (at the very earliest times) of the total spin magnetization curve is related to the polymer–clay interfacial area available in the matrix, or in other words, the initial slope of the curve is proportional to the polymer–clay interface concentration. Curves of Fig. 8 show that the experimental magnetizations exhibit a reasonably linear dependence vs. the square root of the time (5 ms $< t <$ 50 ms). They show that the samples exhibit distinguishable slopes that range more widely than the clay loadings; thus, it can be expected that the nanocomposites should exhibit different degrees of nanomixing. It is worth noticing that the curves of SAN-25
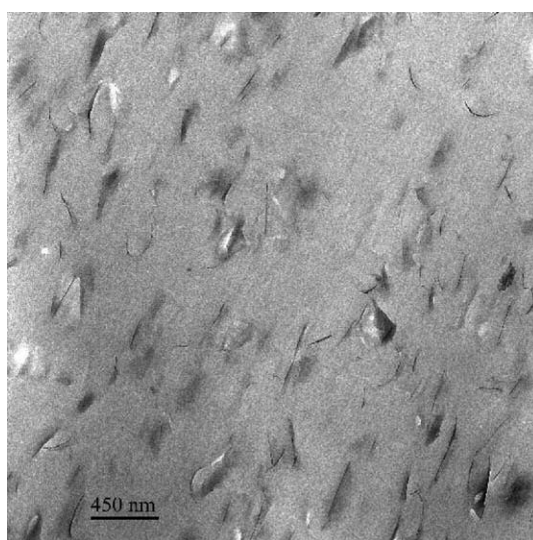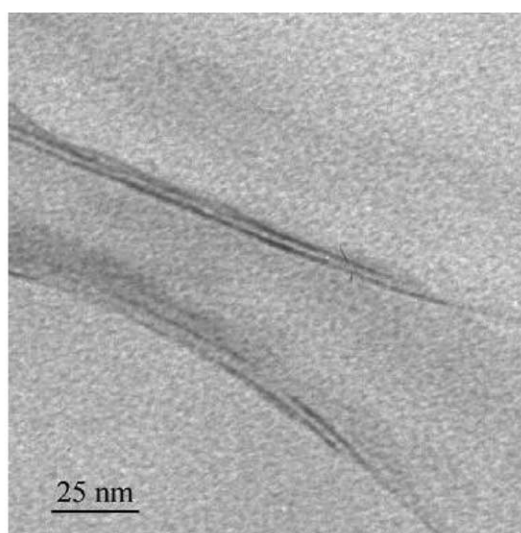
Fig. 4. TEM images at low magnification (a) and high magnification (b) of SAN-25 MMT nanocomposites at 2.2 wt% silicate (average spacing for fully exfoliated, stratified model is 126 nm).
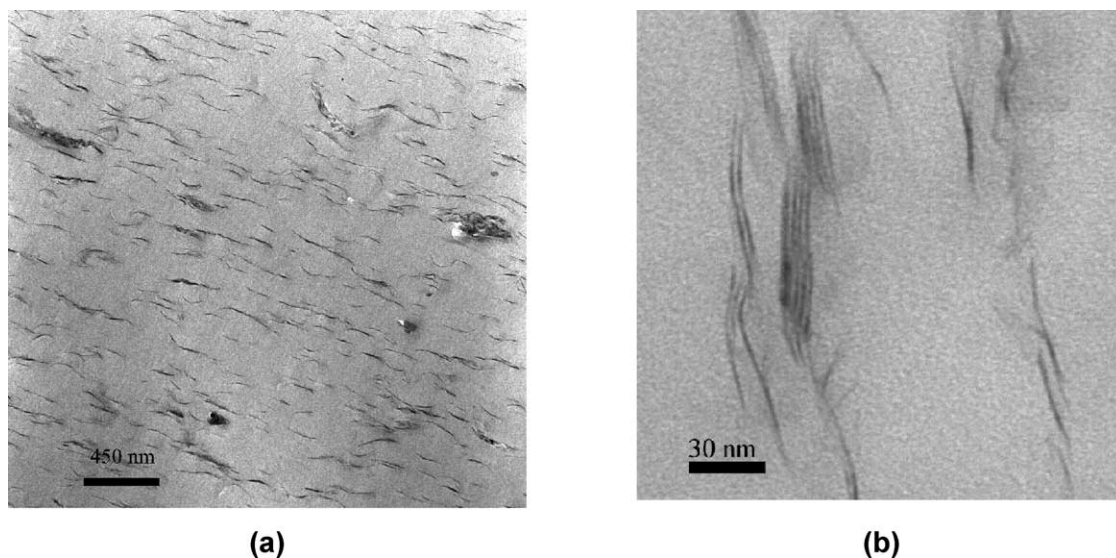
(a) **(b)**

Fig. 5. TEM images at low magnification (a) and high magnification (b) of SAN-25 MMT nanocomposites at 4.2 wt% silicate (average spacing for fully exfoliated, stratified model is 67 nm).

containing 6.2 and 7.9 wt% silicate (noted SAN-25/8 and SAN-25/11 in Fig. 8) exhibit a slight downward curvature, thereby implying that the sample contains galleries smaller than 8 nm (see the calculation in Ref. [17]). This result can be easily explained by the high loading in organoclay favoring the agglomeration of the platelets.

To calculate the fraction of the effective polymer–clay interfacial area, f, from the initial slopes, we need to choose a reference sample which exhibits a fully exfoliated structure. As in our previous work [17], we used a PS/MMT nanocomposite where the organo-modifier of MMT was N,N-dimethyl-n-hexadecyl-(4-vinylbenzyl) ammonium chloride (VB16) and hereafter called PS/VB16 [12]. The important parameter obtained from the reference sample is

$(T_1^H)_S$, which was determined to be 2.5 ms. We also stated that T_{11}^H is a relative indicator of the homogeneity of the distribution of the actual polymer–clay interfaces in the nanocomposite. We can compute, using our model calculation, an apparent spacing, Δ_{app} that matches the T_{11}^H obtained from the experimental curves. We can then compare Δ_{app} with Δ_f, the spacing in an ideally layered structure that has a surface area f times the amount expected from full exfoliation. Thus, we define a parameter, $\varepsilon = \Delta_f/\Delta_{app}$, to be a qualitative monitor of the inhomogeneity of the distribution of clay where poor homogeneity would correspond to $\varepsilon \ll 1$ and good homogeneity would yield $\varepsilon = 1$. The values of f and ε are presented in Table 1.

From the Table 1, we can observe that T_{11}^H's (computed

(a) **(b)**

Fig. 6. TEM images at low magnification (a) and high magnification (b) of SAN-25 MMT nanocomposites at 6.2 wt% silicate (average spacing for fully exfoliated, stratified model is 44 nm).
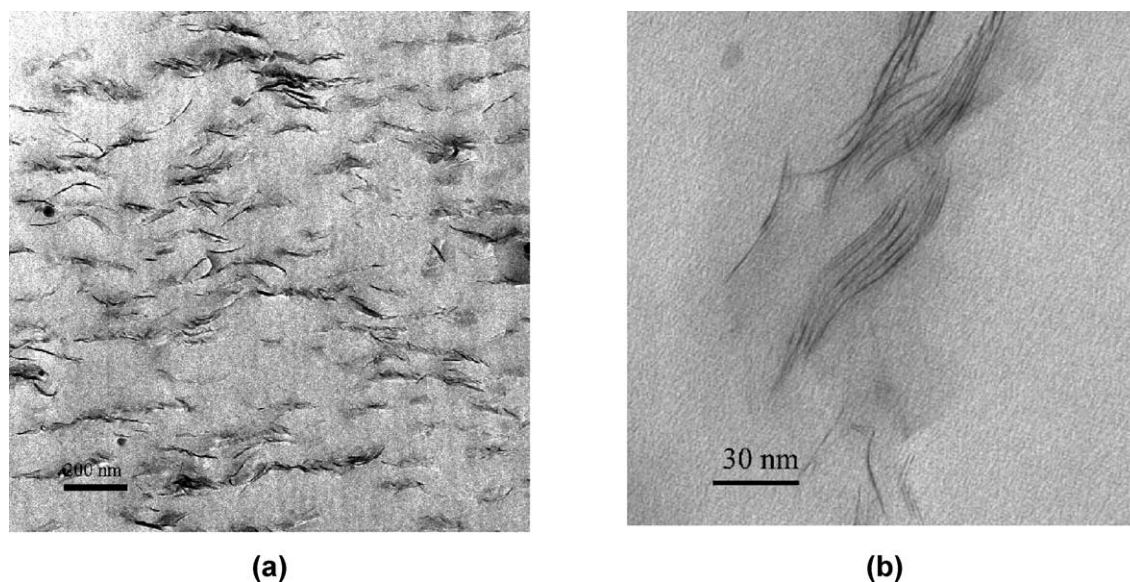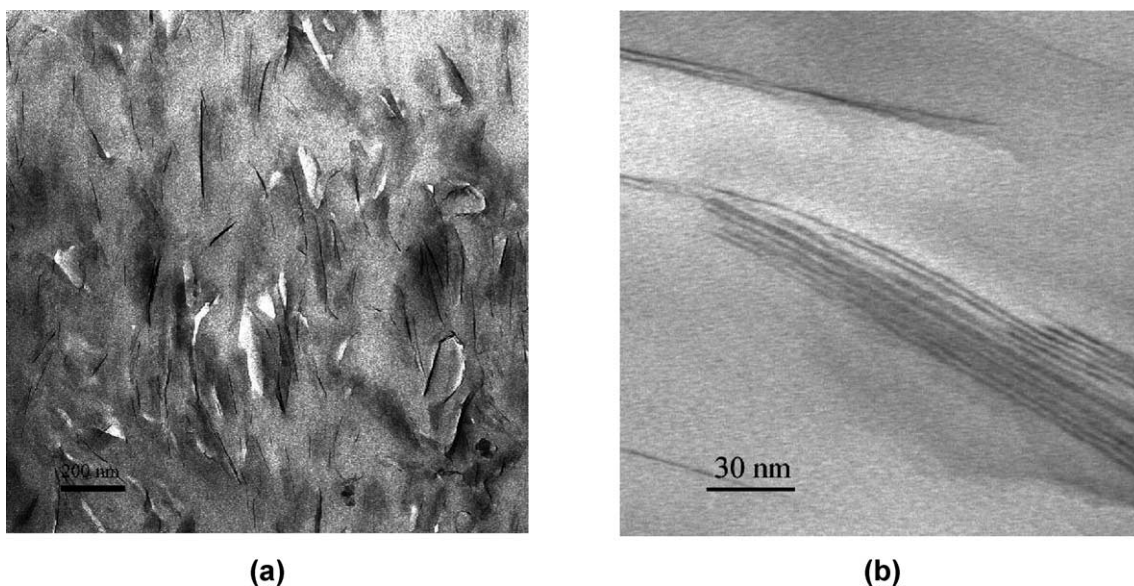
(a)

(b)

Fig. 7. TEM images at low magnification (a) and high magnification (b) of SAN-25 MMT nanocomposites at 7.9 wt% silicate (average spacing for fully exfoliated, stratified model is 35 nm).

by fitting the saturation—recovery curves using Eq. (1)) are significantly shortened, as expected, because of the paramagnetically induced relaxation at the polymer–clay interface (from 20.4 s for pure SAN-25 to 3 s for SAN-25/11) (Fig. 9). By TEM and XRD, SAN-25 MMT nanocomposites are mixtures of intercalated and exfoliated morphologies. By NMR, these samples exhibit f values falling between 0.48 and 0.53, i.e. there is an effective polymer–clay interfacial area of about 0.5. It also is noteworthy that, at the lower clay concentrations, initial slopes of the saturation–recovery curves are pretty linear (Fig. 9). However, at the higher concentrations, there is more of a downward curvature, indicative of increasing numbers of galleries whose separation is in the 3–8 nm range. The latter is in qualitative agreement with the high-magnification TEM

pictures in Figs. 4–7; however, considering the relatively large average gallery spacings indicated in those figure captions (relative to the field of view), one must always be alert to the possibility that the high-magnification images are not completely representative of the whole sample. At the same time, ε values for the SAN-25 MMT nanocomposites cover a range from 34 to 40%, meaning that our nanocomposites show significant inhomogeneity in terms of the distribution of the actual MMT–polymer interfaces.

4.3. T_1^H in the presence of oxygen

It is known from the literature [17,24,25] that the adsorption of paramagnetic oxygen on aromatic polymers causes a major shortening of T_1^H. It was shown for polystyrene but we suspect the same effect for SAN polymer because of the presence of phenyl ring in the repeat unit of this polymer. The amount of adsorbed oxygen
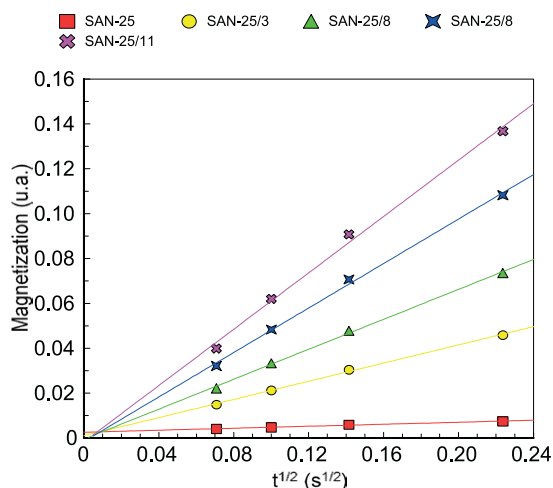

Fig. 8. Magnetization from saturation-recovery experiment vs. the square root of the time of deoxygenated SAN-25/MMT nanocomposites at different loading in organoclay.
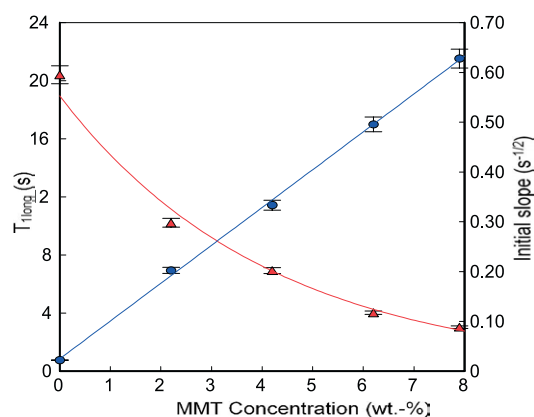

Fig. 9. T_{1l}^H and initial slopes measured from the saturation–recovery curves vs. MMT concentration of deoxygenated SAN-25/MMT nanocomposites at different loading in organoclay.

Table 1
Modified platelet−platelet spacing (Δ) and estimation of the degree of homogeneity in PS/MMT nanocomposites

Polymer	Organo-MMT concentration (wt%)	True silicate concentration (wt%)	T_{1l}^H (s)	f	Δ_f (nm)	Δ_{app} (nm)	ε (%)	TEM/XRD observations
SAN-25	0	0	20.4	0	–	–	–	–
PS/VB16	3.0	2.0	9.7	1.0	136	346	39	Exfoliated
SAN-25/3	3.0	2.2	10.2	0.53	197	496	40	Well and evenly dispersed, exfoliated/intercalated with small tactoids (2/3 layers)
SAN-25/6	5.6	4.2	6.9	0.48	113	322	35	Well and evenly dispersed, exfoliated/intercalated with small tactoids (3/5 layers)
SAN-25/8	8.3	6.2	4.0	0.49	74	208	36	Well and evenly dispersed, exfoliated/intercalated with small tactoids (3/8 layers)
SAN-25/11	10.6	7.9	3.0	0.49	57	172	34	Well and evenly dispersed, exfoliated/intercalated with small tactoids (3/10 layers)

is a function of the chemical nature of the polymer, its molecular packing, molecular motion and temperature. Thus, in addition to the sensitivity of T_1^H to clay dispersion, any other changes that might affect oxygen solubility or dynamics could also influence T_1^H.

Table 2 shows T_1^H data, obtained from τ_{null}, for our oxygen containing SAN-25/MMT nanocomposites. The simplicity of this measurement is most attractive feature; thus we include these data, even though the information content is significantly lower than for the deoxygenated samples.

Contrast in T_1^H for pure SAN-25 is dramatic, 20.4 s for deoxygenated samples and 1.77 s for oxygenated SAN-25. Polystyrene showed a similar paramagnetic effect of oxygen. Nevertheless, T_1^H's of oxygen containing samples, defined as T_1^H(ox), are measurably shortened by the paramagnetic character of the clay even if the relative effect is not nearly as large as for deoxygenated samples.

All the T_1^H(ox) data of SAN-25/MMT nanocomposites fall in between 1.14 and 0.54 s (T_1^H(ox) of the pure SAN-25 is 1.77 s). A monotonic decrease in T_1^H with increasing MMT concentration is observed for all nanocomposites

indicating, qualitatively, that the average gallery spacing is decreasing as the MMT concentration increases. The information content of this τ_{null} measurement is not as high as that from f and ε since the shorter T_1^H limits the time that paramagnetically induced relaxation can be followed. Moreover, τ_{null}, while expected to be related to dispersion, does not distinguish between the degree to which interfaces have been generated and the homogeneity of that distribution. Yet, the monotonic behavior of T_1^H with clay concentration indicates that there are no sudden decreases in the quality of dispersion. We can compare the observed τ_{null} values against those calculated, τ_{null}(opt), from the idealized fully-exfoliated, completely-stratified model. These ratios are given in Table 2, and, as expected, the ratios are greater than one, suggesting that the clay is not dispersed in an optimum manner. In that sense, there is qualitative agreement between the samples with and without oxygen. It should be noted that besides having a lower information content, the use of T_1^H(ox) as a measure of dispersion also involves the assumption that in the polymer, oxygen solubility is exactly what it is in the pure polymer. This is not necessarily so, as was discovered in our previous work

Table 2
NMR, XRD and TEM characterization of oxygenated SAN-25/MMT nanocomposites

Polymer/MMT nanocomposite	True silicate concentration (wt%)	T_1^H(ox) (τ_{null}/ln 2) (s)	τ_{null}/τ_{null}(opt)	XRD/TEM observations
PS	0	1.68	–	–
PS/VB16	2.0	1.12	–	Exfoliated
SAN-25	0	1.77	–	–
SAN-25/3	2.2	1.14	1.3	Well and evenly dispersed, exfoliated/intercalated with small tactoids (2/3 layers)
SAN-25/6	4.2	0.84	1.8	Well and evenly dispersed, exfoliated/intercalated with small tactoids (3/5 layers)
SAN-25/8	6.2	0.63	2.2	Well and evenly dispersed, exfoliated/intercalated with small tactoids (3/8 layers)
SAN-25/11	7.9	0.54	2.5	Well and evenly dispersed, exfoliated/intercalated with small tactoids (3/10 layers)

Table 3
Tensile properties of SAN-25/MMT nanocomposites

Polymer	Silicate concentration (wt%)	Young's modulus (GPa)	Tensile strength (MPa)	Strain at break	TEM/XRD observations
SAN-25	0	3.2	67	2.6	–
SAN-25/3	2.2	4.0	59	1.7	Well and evenly dispersed, exfoliated/intercalated with small tactoids (2/3 layers)
SAN-25/6	4.2	4.6	46	1.1	Well and evenly dispersed, exfoliated/intercalated with small tactoids (3/5 layers)
SAN-25/8	6.2	5.7	41	0.8	Well and evenly dispersed, exfoliated/intercalated with small tactoids (3/8 layers)
SAN-25/11	7.9	6.3	36	0.7	Well and evenly dispersed, exfoliated/intercalated with small tactoids (3/10 layers)

on PS/MMT nanocomposites [17]. There we found that the presence of residual monomer modifies the solubility of oxygen, probably by displacement, thereby influencing $T_1^H(ox)$. In these SAN-25 samples, we checked for the existence of residual monomer and it was undetectable. Also, the level of other small molecules, with high mobilities and possibly short T_1^H's, was also monitored and found to be insignificant; thus the observed values of $T_1^H(ox)$ (and of T_1^H in the case of small-molecule impurities) should be free of such complications. Therefore, in these samples, we have confidence that the observed effects on relaxation times can be attributed to clay paramagnetism.

4.4. Tensile properties

Table 3 shows the tensile properties of SAN-25/MMT nanocomposites. It can be observed that Young's modulus increases as a function of the MMT concentration but concurrently, tensile strength and strain at break decrease. Young's modulus of SAN-25/MMT nanocomposites is substantially superior to that of neat SAN-25 due to the reinforcement of the clay platelets.

The modulus exhibits a linear behavior vs. the MMT content in the polymer (Fig. 10). Surprisingly, tensile strength drops with higher clay loading. Most literature reports show an increase in strength at yield with clay loading [22,28], but the SAN/MMT samples broke in a brittle manner before yield, and comparison to a ductile matrix then is not valid in terms of the strain regime. Both tensile strength and strain at break show a linear decrease at low clay loadings (linear behavior as shown in Fig. 10), suggesting the presence of small agglomerates in the polymer as reported elsewhere [33]. This dependence appears to plateau at higher loadings, but the standard deviation also increases with loading, making the trend difficult to evaluate. The nature of the variation of tensile strength with loading for nanocomposites with a brittle matrix (i.e. SAN) is not completely understood at this time. All nanocomposites exhibit an intermediate structure with some exfoliated platelets as well as tactoids. We also observed a linear dependence of the tensile modulus properties vs. clay content for the range of loading tested. We have, therefore, a 'filler effect' increasing the stiffness but decreasing tensile strength of the nanocomposites.
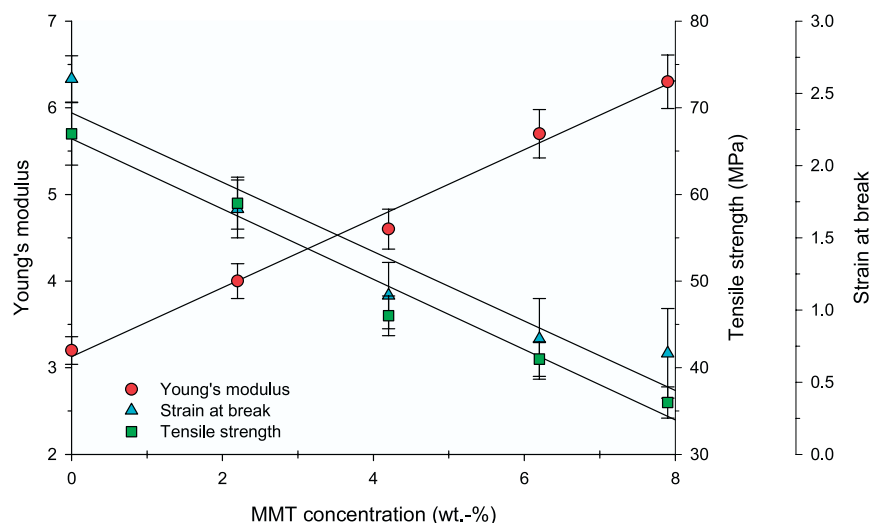

Fig. 10. Young's modulus, tensile strength and strain at break vs. MMT concentration of SAN-25/MMT nanocomposites.
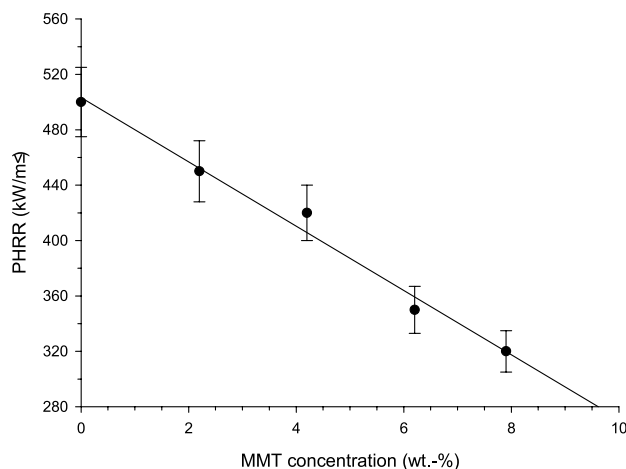
Fig. 11. Peak of heat release rate (PHRR) vs. MMT concentration of SAN-25/MMT nanocomposites.

4.5. Flammability properties

Adding a small amount of clay has been shown to reduce peak of HRR (PHRR) for polystyrene nanocomposites [12, 13], however, to our knowledge, only limited information has been published for melt-processed SAN nanocomposites [34]. Fig. 11 shows significant reductions in PHRR in SAN-25 as a function of clay content. This reduction is strongly enhanced at higher clay loading. As an example, PHRR is decreased by 36% at 4.2 wt% in MMT concentration. The suggested mechanism by which clay nanocomposites function involves the formation of a char that serves as a potential barrier to both mass and energy transport [12]. The higher the concentration of ceramic-like layer that forms at the decomposing surface of the burning sample, the higher the efficiency of the barrier, with due consideration for homogeneity of the forming layer as well.

5. Conclusion

This work has characterized the dispersion of montmorillonite clay in SAN-25 and evaluated the mechanical properties and the reaction to fire of SAN-25/MMT nanocomposites. The nanodispersion is evaluated qualitatively by XRD and TEM, and quantitatively by solid state NMR. SAN-25/MMT nanocomposites reveal an intermediate morphology, an intercalated structure with some exfoliation and with the presence of small tactoids, whatever the loading in MMT is. By NMR, about half of the available polymer–clay interfacial area is formed and the degree of homogeneity characterizing the distribution of this interfacial area is about 40%. The presence of clay in SAN-25 leads to a 'filler effect' whereby the stiffness increases but the tensile strength of the nanocomposites decreases. It also leads to a significant decrease of PHRR measured by mass loss calorimetry.

References

[1] Alexandre M, Dubois P. Mater Sci Eng R 2000;28(1–2):1–63.
[2] Kojima Y, Usuki A, Kawasumi M, Okada A, Fukushima Y, Kurauchi T, Kamigaito O. J Mater Res 1993;8(5):1185–9.
[3] Okada A, Fukushima Y, Kawasumi M, Inagaki S, Usuki A, Sugiyama S, Kurauchi T, Kamigaito O. US Patent 4,739,007; 1988.
[4] Messersmith PB, Giannelis EP. J Polym Sci, A: Polym Chem 1995; 33(7):1047–57.
[5] Gilman JW, Kashiwagi T, Lichtenhan JD. SAMPE J 1997;33:40–6.
[6] Gilman JW. Appl Clay Sci 1999;15(1–2):31–49.
[7] Gilman JW, Kashiwagi T, Giannelis EP, Manias E, Lomakin S, Lichtenhan JD, Jones P. In: Le Bras M, Camino G, Bourbigot S, Delobel R, editors. Fire retardancy of polymers—the use of intumescence. Cambridge: The Royal Society of Chemistry; 1998. p. 223–35.
[8] Jeon HG, Jung HT, Lee SD, Hudson S. Polym Bull 1998;41(1):107–13.
[9] Gilman JW, Jakson CL, Morgan AB, Harris RH, Manias E, Giannelis EP, Wuthenow M, Hilton D, Philips SH. Chem Mater 2000;12:1866–73.
[10] Devaux E, Bourbigot S, El Achari A. J Appl Polym Sci 2002;86: 2416–23.
[11] Lan T, Kaviratna PD, Pinnavaia T. J Chem Mater 1994;6(5):573–5.
[12] Zhu J, Morgan AB, Lamelas FJ, Wilkie CA. Chem Mater 2001;13: 3774–80.
[13] Zhu J, Uhl FM, Morgan AB, Wilkie CA. Chem Mater 2001;13: 4649–54.
[14] Gilman JW, Kashiwagi T, Morgan AB, Harris R, Brassel L, Landingham M, Jackson C. NISTR 2000;6531.
[15] Bourbigot S, Gilman JW, Davis RD, Vanderhart DL, Wilkie CA, Morgan AB. In: Recent advances in flame retardancy of polymeric materials. The Fourteenth Annual BCC Conference on Flame Retardancy, Stamford, CT.
[16] Morgan AB, Gilman JW. J Appl Polym Sci 2003;87(8):1329–38.
[17] Bourbigot S, VanderHart DL, Gilman JW, Awad WH, Davis RD, Morgan AB, Wilkie CA. J Polym Sci, B: Polym Phys 2003;41(24): 3188–213.
[18] VanderHart DL, Asano A, Gilman JW. Macromolecules 2001;34: 3819–22.
[19] VanderHart DL, Asano A, Gilman JW. Chem Mater 2001;13: 3781–95.
[20] VanderHart DL, Asano A, Gilman JW. Chem Mater 2001;13: 3796–809.
[21] Stretz H. Preliminary proposal 2002. Austin: University of Texas; 2002.
[22] Fornes T, Yoon PJ, Keskkula H, Paul DR. Polymer 2001;42:9929–40.
[24] Capitani D, De Rosa C, Ferrando A, Grassi A, Segre AL. Macromolecules 1992;25:3874–80.
[25] Capitani D, Segre AL, Blicharski JS. Macromolecules 1995;28: 1121–8.
[26] Farrar TC, Becker ED. Pulse and Fourier transform NMR. New York: Academic Press; 1971.
[27] Grand A. Heat release calorimetry evaluation of fire retardant polymer systems 42nd International SAMPE Proceedings, vol. 5 1997.
[28] Scudmore MJ, Briggs PJ, Prager FH. Cone calorimetry—a review of tests carried out on plastics for the association of plastic manufacturers in Europe. Fire Mater 1991;15:65–84.

[29] Babrauskas V. development of cone calorimeter—a bench scale rate of heat release based on oxygen consumption NBS-IR 82-2611. Gaithersburg: US Nat. Bur. Stand; 1982.

[30] Babrauskas V. Fire Mater 1984;8(2):81.

[31] VanderHart DL, McFadden GB. Solid State Magn Nucl Res 1996;7: 45–66.

[32] Clauss J, Schmidt-Rohr K, Spiess HW. Acta Polym 1993;44:1–17.

[33] Chang J-H, An YU, Sur GS. J Polym Sci, Part B: Polym Phys 2003; 41:94.

[34] Morgan AB, Chu LL, Anderson SK, Harris JD, Beach MW. Styrene-acrylonitrile (SAN) layered silicate nanocomposites prepared by melt compounding. Polymer 2004;45:4051.